The 9th European Congress on Computational Methods in Applied Sciences and Engineering
ECCOMAS Congress 2024
3–7 June 2024, Lisboa, Portugal

DATA-DRIVEN PERMEABILITY PREDICTION OF 3D FIBROUS MICROSTRUCTURES

DINESH KRISHNA NATARAJAN[1,3], TIM SCHMIDT[2], STEFANO CASSOLA[2], MARLON NUSKE[1], MIRO DUHOVIC[2], DAVID MAY[2], ANDREAS DENGEL[1,3]

[1] German Research Center for Artificial Intelligence (DFKI) GmbH
Trippstadter Str. 122, 67663 Kaiserslautern, Germany
e-mail: dinesh.natarajan@dfki.de, www.dfki.de

[2] Leibniz-Institut für Verbundwerkstoffe GmbH
Erwin-Schrödinger-Straße 58, 67663 Kaiserslautern, Germany
website: www.ivw.uni-kl.de

[3] University of Kaiserslautern-Landau (RPTU)
Gottlieb-Daimler-Straße, 67663 Kaiserslautern, Germany
website: agd.informatik.uni-kl.de

Key words: Fiber-reinforced polymer composites, Microstructure property prediction, Machine Learning, Deep Learning, Geometry-based permeability prediction

Summary. For the manufacturing process simulation of fiber-reinforced polymer composites, flow simulations have to be performed at multiple spatial scales which govern the flow through the fiber structures. Repetitive multiscale flow simulations are computationally expensive and time-consuming. In order to speed up the multiscale simulation workflow, fast machine learning surrogate models or emulators could be used to replace one or more of the flow simulations. In this work, feature-based emulators and geometry-based emulators are developed using neural networks for predicting the permeability of 3D fibrous microstructures based on a reference dataset (doi:10.5281/zenodo.10047095). The best model achieved a mean relative error of 8.33 % on the test set with a significantly faster inference time compared to a conventional simulator.

1 INTRODUCTION

A fiber-reinforced polymer composite is a composite material in which fibers are dispersed in a continuous polymer matrix. Fiber-reinforced composite materials can be prepared by manufacturing processes such as Liquid Composite Molding (LCM), in which several stacks of dry fiber textile layers are impregnated by a liquid polymer system [1]. The efficient design of such impregnation processes is supported by process simulation. The flow of a liquid polymer through the fiber structure is governed by flow phenomena at different spatial scales spanning from micrometers (microscale) to millimeters (mesoscale) to meters (macroscale). To take into account these multiscale phenomena in the process simulation, individual flow simulations are performed on the different spatial scales and the information is transferred to the corresponding higher spatial scales [2, 3, 4]. The first and vital step in this process simulation is the estimation

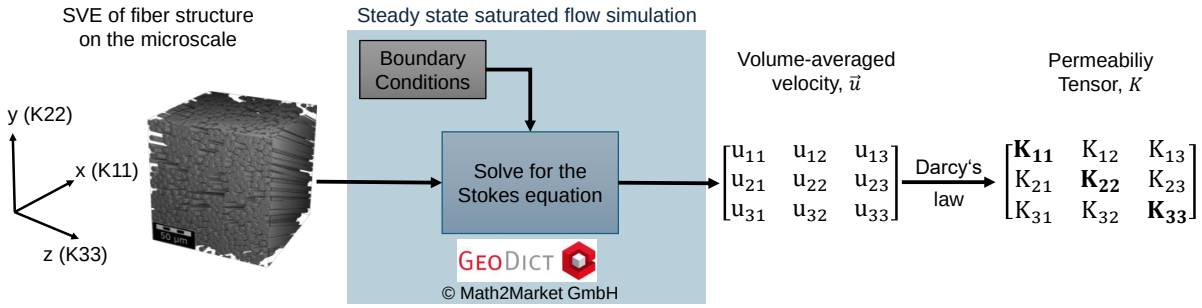

Figure 1: Workflow for numerical permeability prediction for a statistical volume element (SVE) of a 3D fibrous microstructure via steady state saturated flow simulation by solving for the Stokes equation and applying Darcy's law to compute the permeability tensor K.

of permeabilities of the fibrous microstructures. The porous media at higher spatial scales are then subsequently homogenized using the permeabilities of the lower spatial scales.

Presently, conventional methods compute permeability by solving the Stokes equation which governs the fluid flow through the microstructure. However, performing repetitive flow simulations on 3D microstructures require a lot of computational effort and time. Since the flow simulations on higher spatial scales are also expensive, a fast emulator for the permeability prediction on the microscale is desirable. Here, modern machine learning (ML) and deep learning (DL) methods which offer fast inference times have become of great interest. In this work, using a reference dataset [5] generated using a conventional simulator, several ML emulators such as fully connected neural networks (FCNN) and 3D convolutional networks (CNN) are developed to predict the permeability of 3D fibrous microstructures and their performances are comparatively evaluated on a test dataset. Such fast data-driven emulators could be integrated in a multiscale permeability prediction workflow to speed it up.

2 STATE OF THE ART

2.1 PERMEABILITY ESTIMATION

The fluid flow in porous media such as fibrous structures can be described using the Darcy's law [6] shown in Equation 1.

$$\vec{u} = \frac{-K \cdot \Delta p}{\eta \cdot \Delta L} \tag{1}$$

Here $\vec{u}$ is the volume-averaged velocity tensor, K is the permeability tensor, $\Delta p/\Delta L$ is the driving pressure gradient, and η is the dynamic viscosity. The velocity field for a fluid flow through a fibrous microstructure can be determined experimentally [7, 8] or through numerical simulations by solving the Navier-Stokes equation [1] or the further simplified Stokes equations [9] which is shown in Equation 2.

$$-\mu \Delta \vec{u} + \nabla p = \vec{f} \tag{2}$$

The LIR Solver of the commercial software GeoDict (Math2Market GmbH, Germany) which uses the LIR-Tree approach [10] is commonly used for efficient numerical solutions to the Stokes

equation for a 3D voxel structure.

2.2 MACHINE LEARNING FOR PERMEABILITY PREDICTION

In recent years, ML methods have been used as surrogate models (or) emulators to replace conventional simulators for the purpose of permeability prediction of microstructures. The different methods in literature can be classified into two: (1) feature-based methods and (2) geometry-based methods. In the feature-based methods [11, 12, 13], the inputs to the ML models are morphological descriptors about the microstructure such as volume content, porosity, Minkowski functionals, etc. With this approach, the descriptors can be used as input features to classical regression models or FCNN models in order to predict the permeability values. However, such methods necessitate the extraction of morphological features from the microstructure, which could be computationally expensive. The geometry-based methods predict the permeability using either 2D images [14, 15] or 3D images [11, 16] or point clouds [17] of the microstructure as inputs. To the best of our knowledge, the 3D geometry-based ML methods in literature only consider isotropic microstructures to predict the in-flow permeability, whereas our methods consider anistropic fibrous microstructures and predict the diagonal of the permeability tensor.

3 ABOUT THE DATASET

Parameter	Parameter space	Unit
Fiber volume content	50, 52, 54, 56, 58, 60, 62, 64, 66	%
Fiber diameter	6, 7, 8, 9, 10, 11, 12	µm
Fiber direction	0, 11.25, 22.5, 33.75, 45	°

Table 1: The three primary modeling parameters and their parameter spaces which were used to generate the statistical volume elements (SVE) of the 3D fibrous microstructures

The representative dataset [5] of 3D fibrous microstructures and their numerically computed permeabilities created by [18] was at the core of this study. The geometries of the microstructures were artificially generated using FiberGeo module of GeoDict [19]. Three primary features influencing permeability: fiber volume content, fiber diameter and fiber direction were sampled from the parameter spaces defined in Table 1 to generate 4284 geometries as shown in Figure 2. For each of these microstructurs, steady state saturated flow simulations along the three flow directions X, Y and Z were performed using the FlowDict module of GeoDict [20] and the corresponding permeability tensor was calculated using Darcy's Law [6] as illustrated in Figure 1. Further details about the dataset generation can be found in [5, 18]. In this study, the focus was on the task of predicting the diagonal of the permeability tensor for a given 3D fibrous microstructure.

4 MODELING APPROACHES

In this work, two types of ML-based modeling approaches to predict the permeability of 3D fibrous microstructures were considered: (1) Feature-based emulators and (2) Geometry-based emulators. These two approaches had the same task of predicting the diagonal of the permeability tensor, but differed by the input features used to achieve that task.

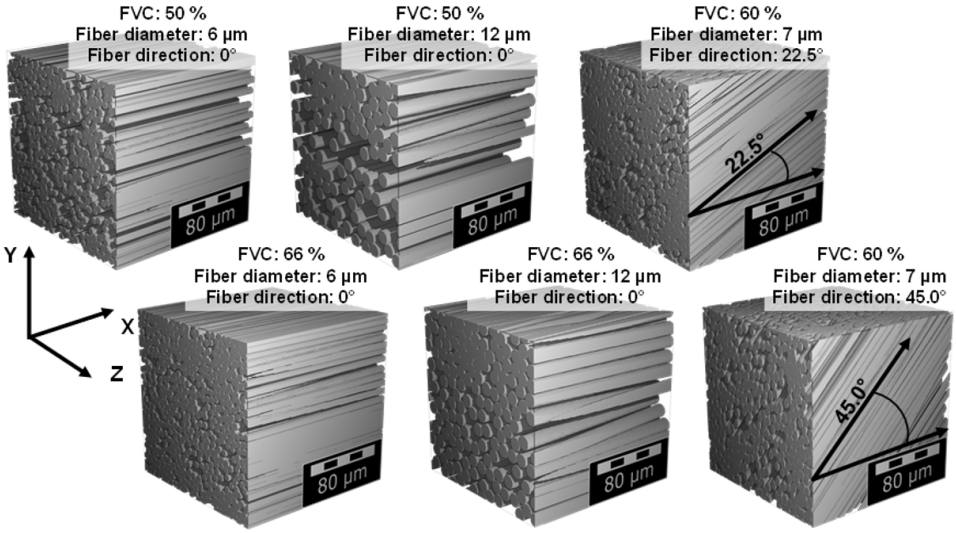

Figure 2: Artificially generated statistical volume elements (SVEs) of the fibrous microstructures by varying the fiber volume content (FVC), fiber diameter and fiber direction. Each geometry has a resolution of 0.5 µm^3 / voxel, containing $320 \times 320 \times 320$ voxels. The coordinate system indicates the three orthogonal flow directions X, Y and Z.

4.1 FEATURE-BASED EMULATORS

The feature-based emulators were designed using fully connected neural networks (FCNN) to map the relationship between the morphological features describing the 3D fibrous microstructures and the diagonal of the permeability tensor. In Approach 1, the fiber features from Table 1 used to generate the microstructures were used as input features. In Approach 2, additionally the five Minkowski features of volume fraction, surface area, curvature integral mean and total, and Euler Characteristic extracted using GeoDict [21] were used. These features describe the topology of the pore space [22] in the fibrous microstructures.

4.2 GEOMETRY-BASED EMULATORS

The geometry-based emulators were designed using 3D convolutional layers and fully connected layers to map the relationship between the 3D fiber microstructure and the diagonal of the permeability tensor. Three modeling approaches of the geometry-based emulators were studied as shown in Figure 4. In the first approach, only the 3D geometry was used as input. In the second approach, the 3D geometry and the three fiber features (volume content, diameter and direction) were used as inputs. In the third modeling approach, the 3D geometry and all 8 additional features were used as inputs.

As seen in Figure 4, the geometry-based emulator consists of two trainable neural network components: the 3D CNN encoder and the FCNN. The 3D CNN encoder learnt a latent representation of the 3D geometry. This latent encoding was then flattened and optionally concatenated with either 3 or 8 additional input features. A FCNN was then used to map the flattened or concatenated features to the target or predicted features.

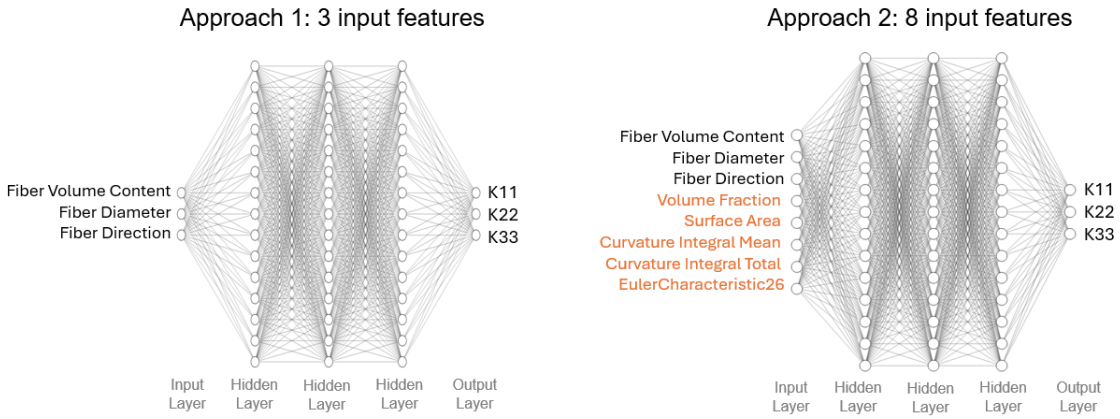

Figure 3: Two modeling approaches for the feature-based emulators: (1) using 3 input features, and (2) using 8 input features to predict the diagonal of the permeability tensor. These emulators were built using configurable FCNNs.

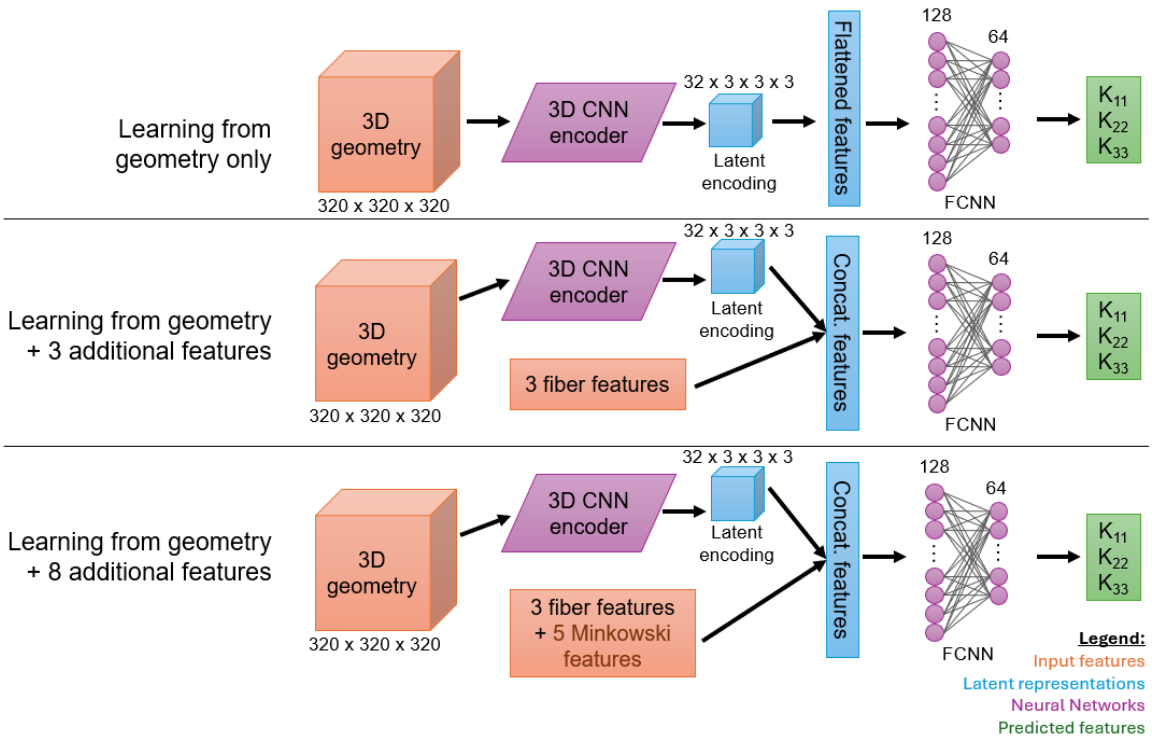

Figure 4: Three modeling approaches for the geometry-based emulators: (a) Using geometry only as inputs, (b) Using geometry and 3 fiber features as inputs, and (c) Using geometry and 8 additional features as inputs to predict the diagonal of the permeability tensor. These emulators were built using 3D CNN encoders and FCNNs. The architecture of the 3D CNN encoders is elaborated in Figure 6.

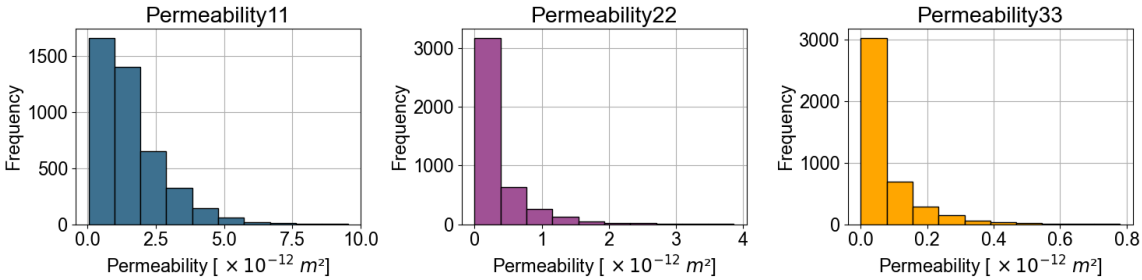

Figure 5: Distributions of the three target permeabilities in the dataset containing 4284 samples. The permeabilities K11, K22, and K33 representing the diagonal of the permeability tensor are each on a different scale with ranges of values between 10^{-12} and $10^{-15}\,m^2$.

5 TRAINING AND EVALUATION

5.1 DATA PROCESSING

For the training of the ML emulators, the dataset of 4284 fiber microstructures and their corresponding permeability values were split into training, validation and test sets using a 60% - 20% - 20% randomized split. To bring the various input features for the feature-based emulators to a similar scale, they were normalized to the range [-1,1]. The 3D geometries were in binary format with 0 values representing voids and 1 values representing fibers, therefore no normalization was applied. The target features, i.e., the diagonal of the permeability tensors in the dataset were each on a different scale with ranges of values between 10^{-12} and $10^{-15}\,m^2$ as shown in Figure 5. Therefore, the three permeabilities were each normalized to the range [-1,1].

5.2 OBJECTIVE FUNCTION

For the regression task of predicting the permeability values, the mean squared error (MSE) was used as the objective function to compute the error between the ground truth and the predictions of the neural network as shown in Equation 3. The errors and their gradients were used to update the neural network parameters using the Adam optimizer [23, 24] with a given learning rate.

$$\mathrm{MSE}(y_{true}, y_{pred}) = \frac{1}{n}\sum_{i=0}^{n}(y^i_{true} - y^i_{pred})^2 \tag{3}$$

where y^i_{true}, y^i_{pred} are the ground truth and predicted permeability values of the i^{th} sample in the normalized scale $[-1, 1]$.

5.3 HYPERPARAMETER TUNING

To find the best FCNN configurations for the feature-based emulators, a hyperparameter search was performed using the Optuna [25] library. Based on the defined search spaces in Table 2, 200 sampling trials were done and subsequent training of the FCNNs were performed to find the best performing model w.r.t MSE on the validation set. The configurations of the best FCNNs for the two modeling approaches for the feature-based emulators are shown in Table 3.

Hyperparameter name	Hyperparameter search space
Number of hidden layers	1,2,3,4
Number of neurons in each hidden layer	logarithmic space in range (4,64)
Activation function	ReLU, LeakyReLU, ELU, SELU, sigmoid, tanh
Dropout rates	0.1, 0.2, 0.3, 0.4, 0.5

Table 2: Hyperparameters of the FCNNs in the feature-based emulators and their search spaces used for the purpose of hyperparameter tuning using Optuna [25].

Hyperparameter	Approach 1: 3 input features	Approach 2: 8 input features
Number of hidden layers	2	3
Layers of the network	[3, 49, 59, 3]	[8, 64, 49, 45, 3]
Activation function	Leaky ReLU	ELU
Dropout rate	0.1	0.2

Table 3: Best performing FCNN configurations based on hyperparameter tuning using Optuna [25] for the two modeling approaches of the feature-based emulators.

The design of the geometry-based emulators were inspired by the architecture proposed by [26]. Different architecture variations from [26] were created by introducing additional input features (Figure 4) and by using different convolutional kernel sizes (Figure 6). The performances of architectures A and B for the three modeling approaches were compared.

5.4 ERROR METRICS

The permeability values predicted by the trained emulators were evaluated in their true scale using the two error metrics: mean relative error (MRE) and coefficient of determination (R^2), which are defined in Equations 4 and 5.

$$\mathrm{MRE}(Y_{true}, Y_{pred}) = \frac{1}{n}\sum_{i=0}^{n}\frac{\left\|Y^i_{true} - Y^i_{pred}\right\|_2}{\left\|Y^i_{true}\right\|_2} \tag{4}$$

$$\mathrm{R^2}(Y_{true}, Y_{pred}) = 1 - \frac{\sum_{i=0}^{n}\left\|Y^i_{true} - Y^i_{pred}\right\|_2}{\sum_{i=0}^{n}\left\|Y^i_{true} - Y_{mean}\right\|_2} \tag{5}$$

where Y^i_{true} is the ground truth permeability values of the i^{th} sample, Y^i_{pred} is the predicted permeability values of the i^{th} sample, and Y_{mean} is the mean permeability values across all samples in the true scale $[m^2]$.

6 RESULTS & DISCUSSION

In this section, the performances of the best architectures from each modeling approach in the feature-based and geometry-based emulators are discussed. All the evaluation metrics are reported on the test set, which were hidden from the models during training.

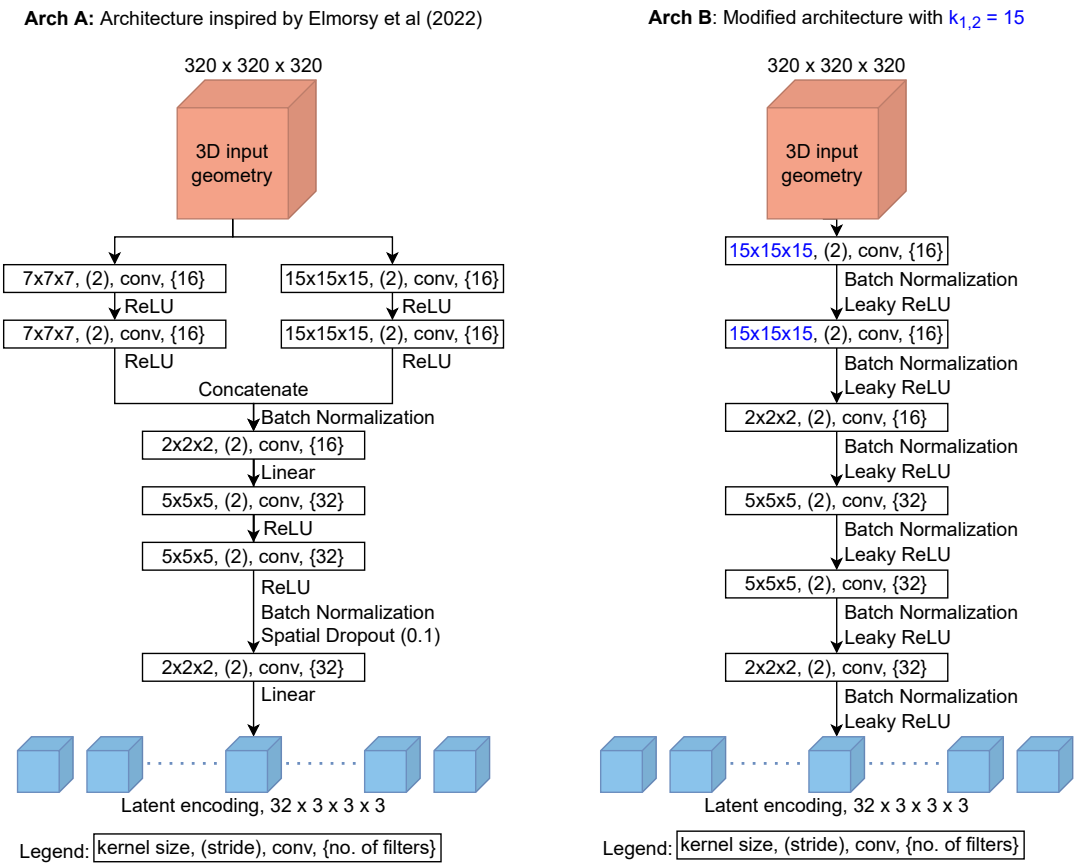

Figure 6: The 3D CNN encoders considered in this study: Architecture A is based on [26] and Architecture B is a modified sequential encoder with variable kernel sizes in the first two layers $k_{1,2}$. Both encoders lead to a latent encoding of dimensions $32 \times 3 \times 3 \times 3$, which was then flattened/concatenated with additional features as described in Figure 4.

In the Table 4, for each modeling approach in the feature-based emulators, the evaluation metrics of the best FCNN model and a baseline ridge regression model are shown. It is observed that the FCNN model clearly outperformed the corresponding ridge regression model for both modeling approaches. On comparing the two modeling approaches, the best FCNN model with 8 input features achieved a lower MRE of 11.35% than the model with 3 input features which had MRE of 12.68%. The R^2 scores for K_{11} and K_{22} were comparable for both models, whereas the model with 3 input features had a slightly better R^2 score for K_{33}.

In the Table 5, the performances of the architectures A and B from Figure 6 for the three modeling approaches of the geometry-based emulators are shown. With respect to both the MRE and R^2 scores, the architecture B with $k_{1,2} = 15$ using geometry and 8 features as inputs clearly outperformed the other architectures with the lowest MRE of 8.33%.

In comparison to the feature-based emulators, improvements were seen in both MRE and R^2 scores for the geometry-based emulators. In particular, the R^2 scores for K_{33} made a significant improvement from 0.706 for the best feature-based emulator to 0.870 for the best geometry-

Modeling Approach	Model	MRE [%]	R^2 score		
		$[K_{11}, K_{22}, K_{33}]$	K_{11}	K_{22}	K_{33}
3 input features	Ridge regression	49.78	0.794	0.681	0.548
	Best FCNN	12.68	**0.941**	0.953	**0.706**
8 input features	Ridge regression	34.14	0.882	0.754	0.622
	Best FCNN	**11.35**	**0.941**	**0.954**	0.701

Table 4: Evaluation metrics for different modeling approaches of the feature-based emulators on the test set. The error metrics compare the ground truth permeabilities and the predicted permeabilities in their true scale $[m^2]$. The lower the MRE metric, the better. The higher the R^2 metric, the better.

Modeling Approach	Architecture	MRE [%]	R^2 score		
		$[K_{11}, K_{22}, K_{33}]$	K_{11}	K_{22}	K_{33}
Geometry only	Arch A	11.21	0.967	0.966	0.818
	Arch B with $k_{1,2} = 24$	13.35	0.942	0.956	0.790
Geometry + 3 features	Arch A	9.48	0.970	0.969	0.818
	Arch B with $k_{1,2} = 24$	9.65	0.978	0.974	**0.870**
Geometry + 8 features	Arch A	12.17	0.973	0.962	0.820
	Arch B with $k_{1,2} = 15$	**8.33**	**0.984**	**0.978**	**0.870**

Table 5: Evaluation metrics for different modeling approaches of the geometry-based emulators on the test set. The error metrics compare the ground truth permeabilities and the predicted permeabilities in their true scale $[m^2]$. The lower the MRE metric, the better. The higher the R^2 metric, the better.

based emulator. Across the 3 modeling approaches, either architecture A or B performed better. Further hyperparameter tuning to find a consistently better performing architecture across the different modeling approaches is necessary.

7 CONCLUSION

In this work, feature-based emulators and geometry-based emulators were developed to predict the diagonal entries of the permeability tensor based on a dataset for permeability estimation of 3D fibrous microstructures [5]. In total, 5 different modeling approaches were trained and then evaluated on an unseen test set. The proposed feature-based and geometry-based emulators can be used as surrogate models to quickly estimate the permeability of a 3D fibrous microstructure. The total computing time used to generate the 4284 samples in the dataset was 1046 hours[i], averaging an inference time of 14.65 minutes per sample. In comparison, the

[i]Using Intel Core i7-8700K, Intel Core i9-12900K CPUs

(a) Best feature-based emulator: 8 input features

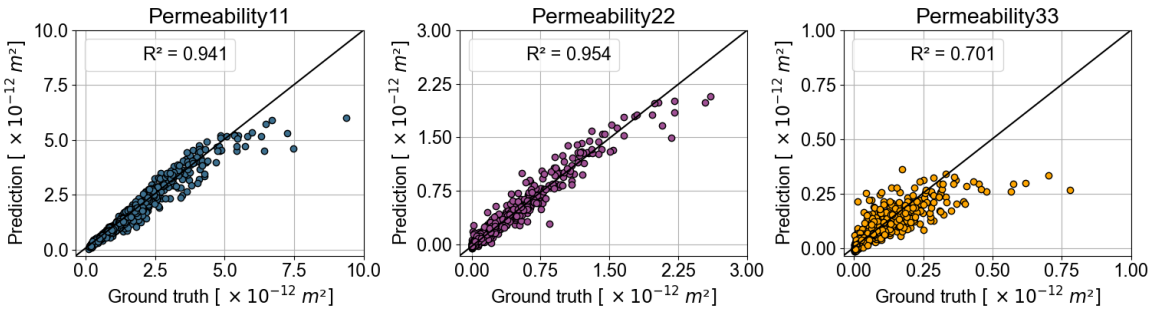

(b) Best geometry-based emulator: Geometry + 8 input features

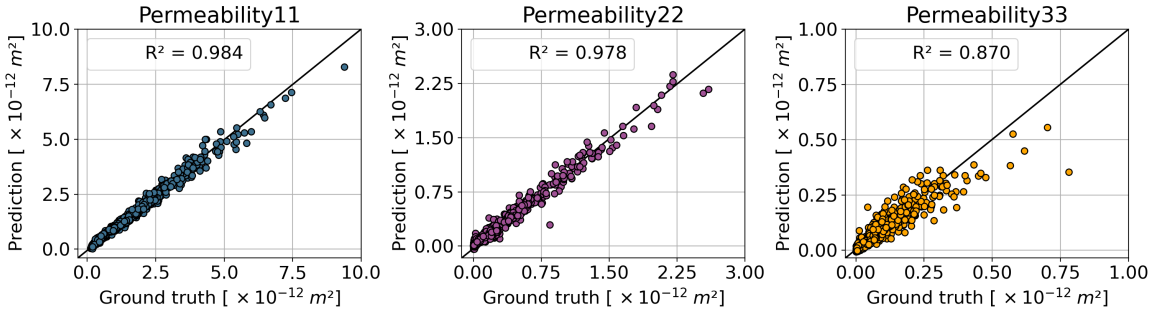

Figure 7: Ground truth vs predicted permeabilities in the true scale on the test set for (a) the best feature-based emulator (using 8 inputs features) and (b) the best geometry-based emulator (using geometry and 8 input features). The solid black diagonal line represents the ideal fit to the data with $R^2 = 1.0$.

training effort and inference times of the proposed emulators are summarized in Table 6. Note that the feature-based models [ii] and geometry-based models [iii] were trained and evaluated using GPUs. Therefore, these fast data-driven emulators can be employed to speed up a multiscale permeability prediction workflow by an order of 10^4 with a relative error of 8.33%.

8 ACKNOWLEDGEMENTS

The project "ML4ProcessSimulation - Machine Learning for Simulation Intelligence in Composite Process Design" is funded by the Leibniz Association within the Leibniz Collaborative Excellence funding program (funding reference: K377/2021).

REFERENCES

[1] David Becker and Peter Mitschang. "Influence of preforming technology on the out-of-plane impregnation behavior of textiles". In: *Composites Part A: Applied Science and Manufacturing* 77 (2015), pp. 248–256. ISSN: 1359-835X. DOI: https://doi.org/10.1016/j.compositesa.2015.05.001.

[ii] Using an NVIDIA GeForce RTX 3070 GPU
[iii] Using an NVIDIA H100 Tensor Core GPU

Model	Time investment		Comparison to simulator	
	Training	Inference per sample	Inference speed-up	Relative Error
Best feature-based emulator	49.31 s	0.14 ms	10^6	11.35 %
Best geometry-based emulator	8.84 h	2.24 ms	10^4	8.33 %

Table 6: Comparison of training and inference times for the proposed feature-based and geometry-based emulators. Significant inference speed-ups are obtained using the emulators while the trade-offs are the relative errors with respect to the simulator.

[2] S. V. Lomov et al. "Textile composites: modelling strategies". In: *Composites Part A: Applied Science and Manufacturing* 32.10 (2001), pp. 1379–1394. ISSN: 1359-835X. DOI: https://doi.org/10.1016/S1359-835X(01)00038-0.

[3] Tim Schmidt et al. "A Novel Simulative-Experimental Approach to Determine the Permeability of Technical Textiles". In: *Key Engineering Materials* 809 (June 2019), pp. 487–492. DOI: 10.4028/www.scientific.net/KEM.809.487.

[4] Tim Schmidt et al. "A combined experimental–numerical approach for permeability characterization of engineering textiles". In: *Polymer Composites* 42 (May 2021). DOI: 10.1002/pc.26064.

[5] Tim Schmidt et al. *Numerically predicted permeability of over 6500 artificially generated fibrous microstructures*. eng. Oct. 2023. DOI: 10.5281/zenodo.10047095.

[6] Henry Darcy. "Les fontaines publiques de la ville de Dijon". In: *Paris: Libraire des Corps Imperiaux des Ponts et Chausses et des Mines* (1856).

[7] D. May et al. "In-plane permeability characterization of engineering textiles based on radial flow experiments: A benchmark exercise". In: *Composites Part A: Applied Science and Manufacturing* 121 (2019), pp. 100–114. ISSN: 1359-835X. DOI: https://doi.org/10.1016/j.compositesa.2019.03.006.

[8] A. X. H. Yong et al. "Out-of-plane permeability measurement for reinforcement textiles: A benchmark exercise". In: *Composites Part A: Applied Science and Manufacturing* 148 (2021), p. 106480. ISSN: 1359-835X. DOI: https://doi.org/10.1016/j.compositesa.2021.106480.

[9] Mahoor Mehdikhani et al. "Voids in fiber-reinforced polymer composites: A review on their formation, characteristics, and effects on mechanical performance". In: *Journal of Composite Materials* 53.12 (2019), pp. 1579–1669. DOI: 10.1177/0021998318772152.

[10] Sven Linden, Andreas Wiegmann, and Hans Hagen. "The LIR space partitioning system applied to the Stokes equations". In: *Graphical Models* 82 (2015), pp. 58–66. ISSN: 1524-0703. DOI: https://doi.org/10.1016/j.gmod.2015.06.003.

[11] Benedikt Prifling et al. "Large-Scale Statistical Learning for Mass Transport Prediction in Porous Materials Using 90,000 Artificially Generated Microstructures". English. In: *Front. Mater.* 8 (Dec. 2021). ISSN: 2296-8016. DOI: 10.3389/fmats.2021.786502.

[12] Jinlong Fu et al. "A data-driven framework for permeability prediction of natural porous rocks via microstructural characterization and pore-scale simulation". en. In: *Engineering*

with Computers 39.6 (Dec. 2023), pp. 3895–3926. ISSN: 1435-5663. DOI: 10.1007/s00366-023-01841-8.

[13] Jianwei Tian et al. "Permeability prediction of porous media using a combination of computational fluid dynamics and hybrid machine learning methods". en. In: *Engineering with Computers* 37.4 (Oct. 2021), pp. 3455–3471. ISSN: 1435-5663. DOI: 10.1007/s00366-020-01012-z.

[14] Baris Caglar et al. "Deep learning accelerated prediction of the permeability of fibrous microstructures". en. In: *Composites Part A: Applied Science and Manufacturing* 158 (July 2022), p. 106973. ISSN: 1359-835X. DOI: 10.1016/j.compositesa.2022.106973.

[15] Jimmy G. Jean, Guillaume Broggi, and Baris Caglar. "An Image-Based Ai Model For Micro-Flow Field Prediction During Resin Transfer Molding: 21st European Conference on Composite Materials". In: *Proceedings of the 21st European Conference on Composite Materials* 5 (2024). Ed. by Christophe Binetury and Frédéric Jacquemin. Place: France Publisher: The European Society for Composite Materials (ESCM) and the Ecole Centrale de Nantes., pp. 753–760. URL: https://doi.org/10.60691/yj56-np80.

[16] Stephan Gärttner et al. "Estimating permeability of 3D micro-CT images by physics-informed CNNs based on DNS". en. In: *Comput Geosci* 27.2 (Apr. 2023), pp. 245–262. ISSN: 1573-1499. DOI: 10.1007/s10596-022-10184-0.

[17] Ali Kashefi and Tapan Mukerji. "Point-Cloud Deep Learning of Porous Media for Permeability Prediction". In: *Physics of Fluids* 33.9 (Sept. 2021). arXiv:2107.14038 [cs, eess], p. 097109. ISSN: 1070-6631, 1089-7666. DOI: 10.1063/5.0063904.

[18] Tim Schmidt et al. "Geometric Model Dataset - FiberStructurePerm - and Machine Learning Models for Permeability Prediction of Fibrous Structures". In: *Polymer Composites* (2024). Submitted, In Review.

[19] Janine Hilden, S. Rief, and Barbara Planas. *GeoDict 2023 User Guide: FiberGeo Handbook*. 2023. DOI: 10.30423/userguide.geodict.

[20] Janine Hilden, Sven Linden, and Barbara Planas. *GeoDict 2023 User Guide: FlowDict Handbook*. 2023. DOI: 10.30423/userguide.geodict.

[21] A. Blumer, S. Rief, and Barbara Planas. *GeoDict 2023 User Guide: MatDict Handbook*. 2023. DOI: 10.30423/userguide.geodict.

[22] J. Ohser and F. Mücklich. In: *Practical Metallography* 38.9 (2001), pp. 538–539. DOI: doi:10.1515/pm-2001-380907.

[23] Diederik P. Kingma and Jimmy Ba. *Adam: A Method for Stochastic Optimization*. Jan. 2017. DOI: 10.48550/arXiv.1412.6980.

[24] Sebastian Ruder. *An overview of gradient descent optimization algorithms*. arXiv:1609.04747 [cs]. June 2017. DOI: 10.48550/arXiv.1609.04747.

[25] Takuya Akiba et al. "Optuna: A Next-generation Hyperparameter Optimization Framework". In: *Proceedings of the 25th ACM SIGKDD International Conference on Knowledge Discovery and Data Mining*. 2019.

[26] Mohamed Elmorsy, Wael El-Dakhakhni, and Benzhong Zhao. "Generalizable Permeability Prediction of Digital Porous Media via a Novel Multi-Scale 3D Convolutional Neural Network". en. In: *Water Resources Research* 58.3 (2022), e2021WR031454. ISSN: 1944-7973. DOI: 10.1029/2021WR031454.